UCRL-9539

UNIVERSITY OF CALIFORNIA

Ernest O. Lawrence Radiation Laboratory

DISCLAIMER

UCRL-9539

UNIVERSITY OF CALIFORNIA

Lawrence Radiation Laboratory
Berkeley, California

Contract No. W-7405-eng-48

PION PRODUCTION BY NEGATIVE PIONS

Barry C. Barish, Richard J. Kurz, Paul G. McManigal,
Victor Perez-Mendez, and Julius Solomon

January 23, 1961

PION PRODUCTION BY NEGATIVE PIONS*

Barry C. Barish, Richard J. Kurz, Paul G. McManigal,
Victor Perez-Mendez,† and Julius Solomon

Lawrence Radiation Laboratory
University of California
Berkeley, California

January 23, 1961

The reaction $\pi^- + p \rightarrow \pi^- + \pi^+ + n$ for $T_{\pi \text{ incident}} = 365$ Mev and 432 Mev was studied. In a previous experiment Perkins et al. investigated this reaction.[1] Their total cross section was much larger than predicted by static model theory. Rodberg suggested that the large difference between experiment and theory was explainable by the inclusion of a pion-pion interaction.[2] Perkins also noted a possible deviation of the energy spectrum of the observed pion from a statistical distribution. The significant interactions at these energies are

$$\pi^- + p \rightarrow \pi^- + p + \pi^0 \qquad \text{(1a)}$$

$$\rightarrow \pi^0 + n \qquad \text{(1b)}$$

$$\rightarrow \pi^- + \pi^+ + n \qquad \text{(1c)}$$

$$\rightarrow \pi^- + \pi^0 + p \qquad \text{(1d)}$$

$$\rightarrow \pi^0 + \pi^0 + n\,. \qquad \text{(1e)}$$

The π^+ from Reaction (1c) with 30 Mev $\leq T_{\pi^+} \leq 180$ Mev was observed at $\theta = 20$, 50, 80, and 110 degrees. The energy of the π^+ was determined by a magnetic spectrometer.

The π^- incident beam was produced by the primary proton beam of the Berkeley 184-inch synchrocyclotron striking an internal Be target. A doublet quadrupole magnet located inside the shielding of the accelerator was used

*Work done under the auspices of the U. S. Atomic Energy Commission.

†Present address: Hebrew University, Jerusalem, Israel.

astigmatically to compensate the effects of the main field of the machine and yield a parallel beam outside the shielding. The π^- beam was momentum-analyzed by a 40-deg bend in an H magnet and focused at the target by a doublet quadrupole magnet. After collimation the cross section of the beam was 3/4 in. × 1-3/4 in. The properties of the pion beams as determined by range curves and calculations are listed in Table I.

Table I. Properties of π^- beams

Energy (Mev)	Percent μ^-	Percent e^-	Intensity
365 ± 15	4.1	1.0	3×10^6/minute
432 ± 15	3.8	1.0	1×10^6/minute

The liquid hydrogen target was a 4-in.-long 2-in.-diameter Mylar cylinder whose axis lay along the beam direction. The target was constructed so that 300 deg could be viewed in the laboratory, obstructed by only 0.031 in. of Mylar. The experimental arrangement of the target area is shown in Fig. 1. For the spectrometer, a C magnet with 13×24-in. pole pieces and a 4-in. gap (maximum field = 19 kG) was used in a wedge configuration[3] to obtain focusing in the horizontal plane. The π_i, π_i' counters were located at the image of the target for a momentum corresponding to the desired π^+ energy. The energy resolution and solid angle of the π^+ channels were determined to within ±5% by wire-orbit measurements. A π^+ count required a coincidence ($1234\pi_i\pi_i'$). Protons with momentum equal to the π^+ momentum were excluded by appropriate thicknesses of Cu absorber inserted between π_i and π_i'. For the monitor coincidences (12) a fast coincidence (4 nsec resolving time) followed by a 40-Mc transistorized discriminator-

scaler circuit was used. The high π^- beam intensities and cyclotron beam rf fine structure introduced problems in direct counter monitoring of the π^- beam. Therefore, a thin-walled ionization chamber was used as an absolute monitor, and was calibrated versus the (12) coincidences at lower beam intensities. The accuracy of the monitor was ±2% at 365 Mev and ±0.5% at 432 Mev.

Positrons of the proper momentum resulting from

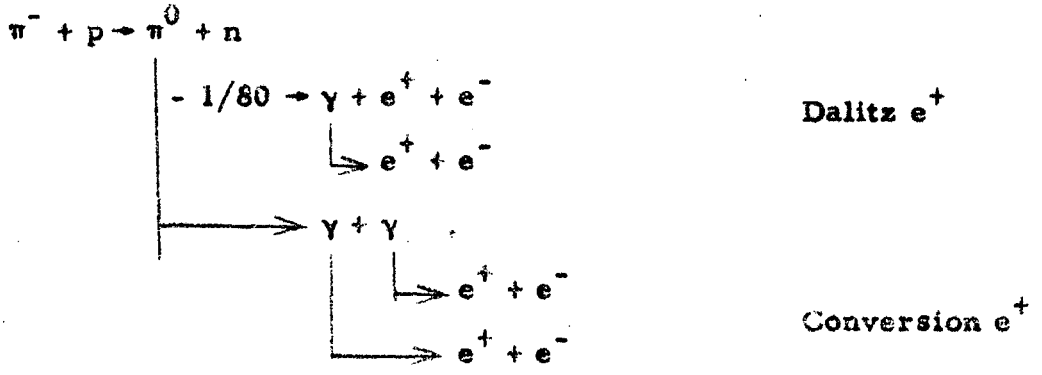

were not excluded by the π^+-detection system. The number of conversion e^+ was experimentally determined by inserting Cu converting material between the target and Counter 3 in multiples of the amount of converting material in the target (≈ 0.01 radiation length). The slope of the plot of yield vs. converting material indicates the number of conversion e^+ entering the spectrometer magnet. These measurements were made at $\theta = 20$ deg for 365 Mev and 432 Mev. The measured values agreed with calculations of $\frac{d^2\sigma}{dEd\Omega}$ for conversion e^+ made using the differential cross section data on $\pi^- + p \rightarrow \pi^0 + n$ by Caris.[4] $\frac{d^2\sigma}{dEd\Omega}$ for Dalitz e^+ was also calculated by using the Caris data and the energy and angular distribution of the Dalitz e^+ in the π^0 rest system.[5] The total positron contamination at $\theta = 20$ deg was ≈ 0.17 at 365 Mev and ≈ 0.12 at 432 Mev. The values decrease rapidly as θ increases. The calculated values were used to correct the data. The efficiency of the π^+ detection system was calculated. Losses of π^+ due to $\pi^+ \rightarrow \mu^+ + \nu$ ($\approx$ 2% to 7%), Coulomb scattering, and nuclear absorption of the π^+ were taken into account.

The results for $\frac{d^2\sigma}{dT^*d\Omega^*}$, $\frac{d\sigma}{d\Omega^*}$, and σ_{total} are presented in Table II. Figure 2 illustrates a typical π^+ energy distribution along with a phase-space statistical distribution normalized to give equal $\frac{d\sigma}{d\Omega^*}$. At 365 Mev $\frac{d\sigma}{d\Omega^*}$ is isotropic. At 432 Mev $\frac{d\sigma}{d\Omega^*}$ was fitted to a curve of the form $a_0 + a_1 \cos\theta^*$. The coefficients a_0, a_1 obtained by the least-squares method are presented in Table III with those of Perkins[1] for comparison.

The total cross sections agree with Perkins et al.[1] and therefore substantiate the experimental deviation from calculations based on static models.[6] The inclusion of a pion-pion interaction by Rodberg[2] produces agreement with the measured total cross sections but predicts a pion energy spectrum favoring higher energies than phase-space statistical distributions. The striking feature of the measured π^+ energy distributions is the low-energy peaking. The laboratory-system energy and angle of the observed π^+ determines ω, the total energy of the π^- and $n(T = 3/2)$ in their barycentric system.[7] The isobar model[8] assumes that final-state π-N combinations in the resonant state ($T = 3/2$, $J = 3/2$, $\omega = 1230$ Mev) are preferred. At our incident π^- energies the total center-of-mass energy available requires a low-energy π^+ if ω is to approach 1230 Mev. The low-energy peaking agrees with the qualitative predictions of the isobar models. In Fig. 2b $\frac{d^2\sigma_{observed}}{d^2\sigma_{phase\ space}}$ is plotted versus ω for all experimental points at both energies. The increase of this ratio in the region of the (3, 3) pion-nucleon resonance is pronounced. Anisovich[9] has presented a model which explains the enhanced total cross section for Reaction (1c) and the strong influence of the (3, 3) resonance on the π^+ differential distributions, using only the resonant pion-nucleon final-state interaction.

We should like to acknowledge the continued interest and support of Professor A. C. Helmholz and Professor Burton J. Moyer. We also wish to thank Mr. James Vale and the cyclotron crew for their assistance and cooperation during the course of the experiment.

Table II. Differential cross sections with respect to π^+ energy and angle; π^+ angle; and total cross sections (*denotes total center-of-mass quantity).

T_π inc. (Mev)	θ(deg)	T^* (Mev)	θ^*(deg)	$d^2\sigma/dT^*d\Omega^*$ (μb/sr-Mev)	$d\sigma/d\Omega^*$ (μb/sr)	σ_T (mb)
365±15	20	35±4.2	33	2.26±0.19	167.7±13.5	2.07±0.09 ?
		48±6.0	31.5	2.04±0.17		
		65.5 ±6.8	31	1.48±0.13		
		83.5 ±8.2	30.5	1.00±0.08		
	50	37.5 ±4.3	78.5	2.17±0.16	174.1±13.0	
		52.5 ±4.8	75.3	2.05±0.15		
		70.2 ±7.0	73	1.53±0.11		
		87.3 ±8.6	71.5	1.27±0.09		
		105 ±11.5	70.5	0.77±0.06		
	80	37.5 ±1.2	116	1.87±0.23	148.4±13.7	
		53.7 ±3.2	109	1.99±0.15		
		71.0 ±5.3	107.5	1.29±0.09		
		96.2 ±6.1	105	0.69±0.06		
		115.0 ±5.1	104	0.45±0.05		
	110	53.0 ±2.5	138	2.29±0.31	167.6±16.5	
		76.1 ±4.3	135	1.82±0.13		
		96.0 ±7.2	133	0.98±0.08		
		115.0 ±4.5	132	0.73±0.08		
432±15	20	19.5 ±3.3	37	3.11±0.33	297.1±24.1	3.26±0.14
		35.0 ±4.3	34.5	3.81±0.32		
		53.0 ±6.1	33	3.67±0.27		
		69.5 ±8.5	32	2.46±0.20		
		90.0 ±8.5	31	1.51±0.14		

Table II (Cont.)

T_π inc. (Mev)	θ(deg)	T^* (Mev)	θ^*(deg)	$d^2\sigma/dT^*d\Omega^*$ (μb/sr-Mev)	$d\sigma/d\Omega^*$ (μb/sr)	σ_T (mb)
	50	35.0 ±4.0	83	3.21±0.24	276.6±21.9	
		51.5 ±5.0	78	2.74±0.21		
		68.7 ±8.5	74.5	2.88±0.20		
		86.5 ±8.3	73	2.21±0.16		
		115.3 ±9.7	72	0.81±0.08		
	80	38.5 ±2.3	116	2.20±0.27	238.6±21.7	
		61.0 ±3.6	110	3.16±0.25		
		79.3 ±5.5	108	2.47±0.18		
		101.0 ±7.5	106	1.76±0.13		
		117.3 ±8.8	105	0.95±0.09		
	110	58.2 ±3.2	132.5	2.17±0.21	232.0±23.4	
		81.0 ±4.3	131.5	2.04±0.16		
		101.5 ±5.5	130.6	1.88±0.14		
		126.8 ±9.0	130.5	0.85±0.07		
		146.7 ±5.0	130.5	0.56±0.09		

Table III. Least-squares-fit coefficients for $\frac{d\sigma}{d\Omega^*} = a_0 + a_1 \cos \theta^*$ at $T_{\pi^- \text{incident}} = 432$ Mev.

	a_0(μb/sr)	a_1(μb/sr)
This experiment	259.3 ± 11.3	46.9 ± 20.6
Perkins et al.	267.7 ± 20.4	137.7 ± 36.3

References

1. W. A. Perkins, J. C. Caris, R. W. Kenney, L. Knapp, and V. Perez-Mendez, Phys. Rev. Letters 3, 56 (1959);
   W. A. Perkins, J. C. Caris, R. W. Kenney, and V. Perez-Mendez, Phys. Rev. 118, 1364 (1960).
2. L. S. Rodberg, Phys. Rev. Letters 3, 58 (1959).
3. W. G. Cross, Rev. Sci. Instr. 22, 717 (1951).
4. J. C. Caris, R. W. Kenney, V. Perez-Mendez, and W. A. Perkins, Charge-Exchange Scattering of Negative Pions by Hydrogen at 230, 260, 290, 317, and 371 Mev (submitted to Phys. Rev.)
5. R. H. Dalitz, Proc. Royal Soc. (London) A64, 667 (1951).
6. S. Barshay, Phys. Rev. 103, 1102 (1956);
   J. Franklin, Phys. Rev. 105, 1101 (1957);
   L. S. Rodberg, Phys. Rev. 106, 1090 (1957);
   E. Kazes, Phys. Rev. 107, 1131 (1957).
7. G. F. Chew and F. E. Low, Phys. Rev. 113, 1640 (1959).
8. S. J. Lindenbaum and R. M. Sternheimer, Phys. Rev. 109, 1723 (1958);
   S. Bergia, F. Bonsignori, and A. Stanghellini, Nuovo cimento 16, 1073 (1960).
9. V. V. Anisovich, Soviet Physics—JETP 12, 71 (1961).

LEGENDS

Fig. 1. Diagram of hydrogen target and counter arrangement.

Fig. 2. (a) $\frac{d^2\sigma}{dT^*d\Omega^*}$ versus $T^*_{\pi^+}$ for T_{π^-} incident = 365 Mev and θ_{π^+} = 50 deg. Solid curve is a phase-space distribution normalized to $\frac{d\sigma}{d\Omega^*}$.

Fig. 2. (b) The ratio of $\frac{d^2\sigma}{dT^*d\Omega^*}$ / observed and normalized $\frac{d^2\sigma}{dT^*d\Omega^*}$ phase space versus ω, the total energy of the π^- and neutron in their barycentric system. The errors indicated include that of $\frac{d^2\sigma}{dT^*d\Omega^*}$ and the uncertainty in the normalization of $\frac{d^2\sigma}{dT^*d\Omega^*}$ phase space.

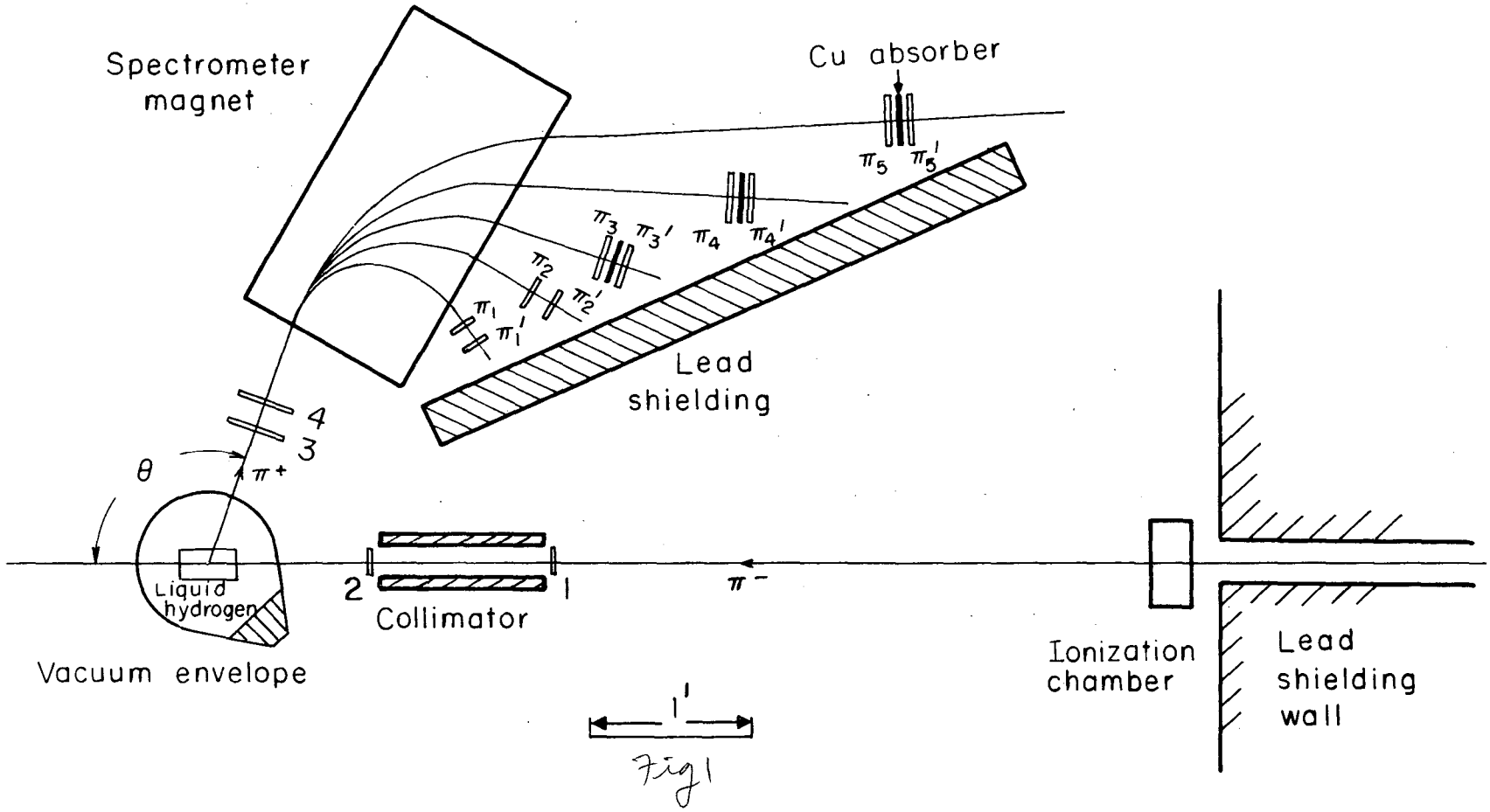
Spectrometer magnet
Cu absorber
π_5 π_5'
π_3 π_3' π_4 π_4'
π_2 π_2'
π_1 π_1'
Lead shielding
4
3
θ
π^+
Liquid hydrogen
Vacuum envelope
2
1
Collimator
π^-
Ionization chamber
Lead shielding wall
1'

Fig 1

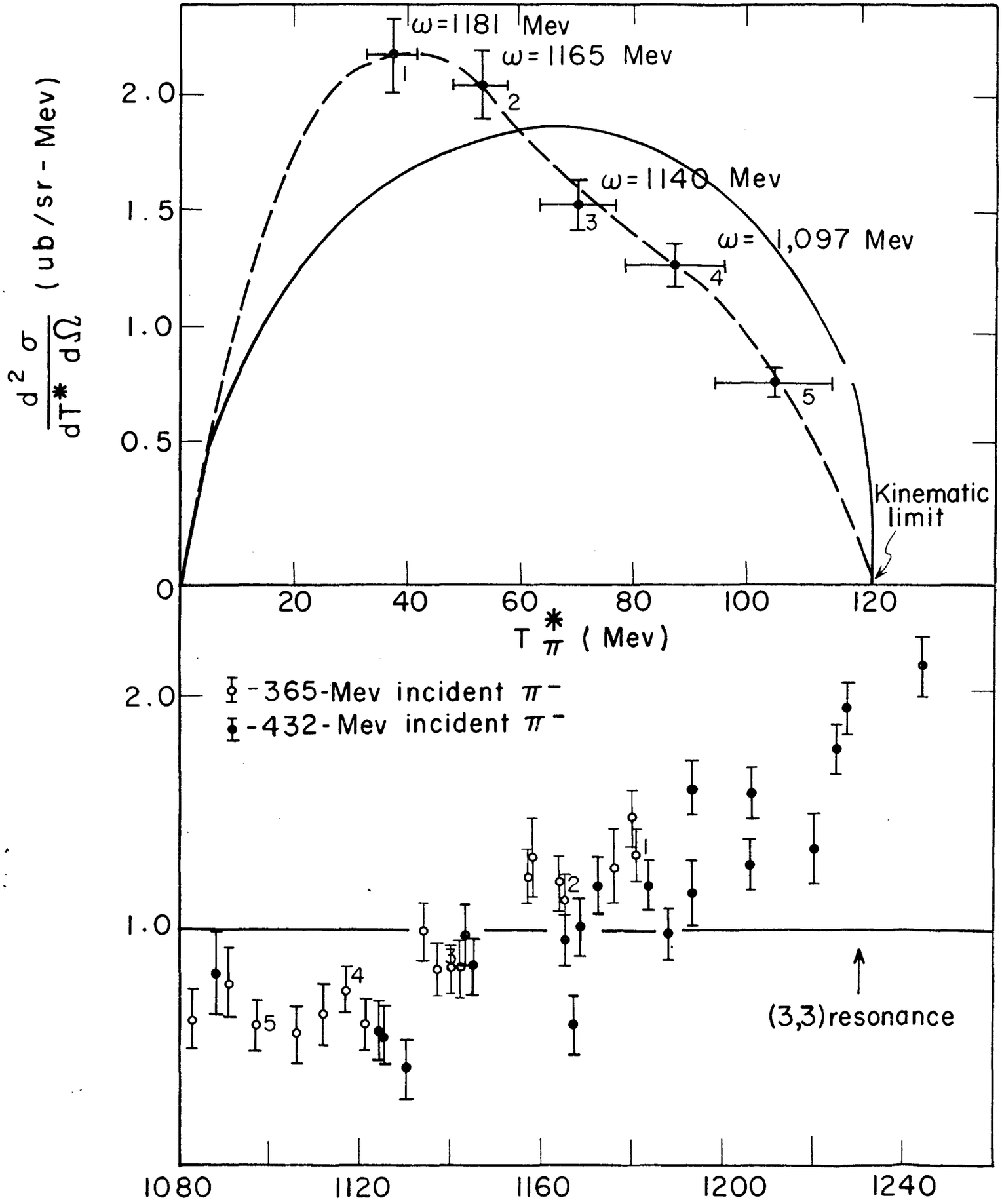
ω=1181 Mev
ω=1165 Mev
ω=1140 Mev
ω= 1,097 Mev
Kinematic limit
$\frac{d^2\sigma}{dT^* d\Omega}$ (ub/sr - Mev)
T_π^* (Mev)
-365-Mev incident π⁻
-432-Mev incident π⁻
(3,3)resonance
0
0.5
1.0
1.5
2.0
20
40
60
80
100
120
1080
1120
1160
1200
1240